ELSEVIER

Fluid Dynamics Research 22 (1998) 191–213

FLUID DYNAMICS RESEARCH

Viscous evolution of 2D dipolar vortices

J.H.G.M. van Geffen[a,*], G.J.F. van Heijst[b]

[a] *Geophysical and Environmental Fluid Dynamics Laboratory, Department of Civil Engineering, University of Dundee, Nethergate, Dundee DD1 4HN, UK*

[b] *Fluid Dynamics Laboratory, Department of Applied Physics, Eindhoven University of Technology, P.O. Box 513, 5600 MB Eindhoven, The Netherlands*

Received 14 March 1997; revised 18 August 1997; accepted 18 August 1997

Abstract

Numerical simulations with a finite-difference method have revealed that a Lamb dipole when placed in a viscous fluid moves along a straight line with decreasing velocity and increasing radius. The relationship between vorticity and streamfunction, which initially is linear, becomes more and more sinh-like as the dipole decays. Some other initial dipolar vorticity distributions (like two oppositely signed monopolar vortices) were found to evolve to a dipolar structure with Lamb-like characteristics. © 1998 The Japan Society of Fluid Mechanics Incorporated and Elsevier Science B.V. All rights reserved.

PACS: 47.32.Cc; 47.11.+j
Keywords: Vortex dynamics; Computational methods in fluid dynamics

1. Introduction

Two-dimensional (2D) turbulence shows, unlike three-dimensional turbulence, the emergence of large-scale structures from small(er)-scale structures; see e.g. McWilliams (1984). This process of self-organisation in 2D turbulence finds its origin in the inverse energy cascade: energy initially distributed over all scales eventually ends up in the large scales and thus coherent vortex structures are formed. The most common type of such structures that have been found to form is the monopolar vortex. Dipolar vortices are common too, though they are less frequently observed than monopoles. A tripolar vortex structure has also been seen to form (see e.g. Legras et al., 1988). In the present study the attention is restricted to dipolar vortices.

If, for instance, a turbulent blob of dye is injected horizontally at the appropriate density level in a stratified fluid (the stratification suppresses vertical motions and thus tends to make the flow quasi-2D), this blob collapses to a flat pancake-like structure which consists of two closely packed patches of oppositely signed vorticity (Van Heijst and Flór, 1989; Flór and Van Heijst, 1994). The

* Corresponding author. E-mail: jos@tnj.phys.tue.nl.

PII S0169-5983(97)00033-6

vertical dimension of such a dipole is much smaller than its horizontal size, hence it can be treated as a planar, quasi-2D structure. Similar dipolar vortices can be created by towing a cylinder through a rotating fluid (in which the rotation of the fluid provides the two-dimensionalizing mechanism of the motions; Velasco Fuentes and Van Heijst, 1994) or through a thin soap film (Couder and Basdevant, 1986): the flow in the wake of the cylinder consists of one or more dipolar vortices. Electric pulses in a layer of mercury, which is subjected to a magnetic field to make the motions 2D, can also lead to the formation of dipolar vortices (Nguyen Duc and Sommeria, 1988).

The dipole formed in these 2D flows is fairly stable: the vortex retains its dipolar structure during its motion (caused by the dipole's net linear momentum), even though the dipole gradually decays due to viscous effects, as discussed e.g. by Flór and Van Heijst (1994) and Flór et al. (1995). Under geophysical circumstances dipolar vortices are often disturbed or even torn apart by external forces, such as strain and shear. These effects are not discussed here: the present study focusses on the evolution of dipolar vortices themselves. A numerical and experimental study of the effects of a strain on dipoles has been done by Trieling et al. (1997), and the effects of a shear are the subject of future work.

From the analysis of the dipoles formed in laboratory experiments it appears that its characteristics are well described by the so-called Lamb dipole, a dipolar vortex with a circular form, which is a solution of the inviscid vorticity equation in an infinite domain constructed by Lamb (1932). (In fact, this solution was already formulated in a more general form by Chaplygin (1903); see also Meleshko and Van Heijst (1994).) In an inviscid fluid the Lamb dipole moves along a straight line with constant velocity and without change of form. This paper presents the results of a numerical study of the effects of viscosity and the finiteness of the domain on the evolution of a Lamb dipole. The numerical method used, a finite-difference method, is outlined in the next section. Section 3 presents the Lamb dipole and the results of the numerical simulations of the evolution are discussed in Section 4. Since a dipolar structure with Lamb-like characteristics appears to be a stable structure in 2D turbulence, Section 5 focusses on the (numerical) evolution of some other initial dipolar structures (such as two monopolar vortices of opposite sign next to each other) to study whether a Lamb-like dipolar structure emerges. Some conclusions are formulated in Section 6.

2. The numerical model

This section presents in brief the basic equations that describe the evolution of a two-dimensional vorticity distribution and the numerical method used for the flow simulations.

2.1. Governing equations

The flow field $\boldsymbol{v}$ of an incompressible fluid (i.e. $\nabla \cdot \boldsymbol{v} = 0$) is governed by conservation of momentum, which is described by the Navier–Stokes equation. For two-dimensional (2D) flows $\boldsymbol{v} = (u, v, 0)$ without background rotation or topography, the Navier–Stokes equation may be written in the vorticity-streamfunction formulation:

$$\frac{\partial \omega}{\partial t} + J(\omega, \psi) = \nu \nabla^2 \omega, \tag{1}$$

with the vorticity ω defined as usual by $\boldsymbol{\omega} = \nabla \times \boldsymbol{v} = (0, 0, \omega)$, and the streamfunction ψ by $u = \partial\psi/\partial y$ and $v = -\partial\psi/\partial x$. In Eq. (1) the Jacobian operator $J(\omega, \psi)$ represents the nonlinear advection terms and ν the kinematic viscosity. From their respective definitions it follows that the vorticity is related to the streamfunction by a Poisson-type equation:

$$\omega = -\nabla^2\psi. \tag{2}$$

Eqs. (1) and (2) describe the evolution of a certain vorticity distribution under the influence of nonlinear and viscous effects.

The following quantities are also used in this paper:

$$\begin{aligned} &\text{circulation: } \Gamma = \iint_A \omega \, \mathrm{d}A, \\ &\text{kinetic energy: } E = \frac{1}{2} \iint_A (\nabla\psi)^2 \, \mathrm{d}A, \\ &\text{enstrophy: } H = \frac{1}{2} \iint_A \omega^2 \, \mathrm{d}A, \end{aligned} \tag{3}$$

where $\mathrm{d}A$ is a surface element of the full computational domain A. Often the circulation Γ is split into two parts: Γ_+ for all areas of positive vorticity and Γ_- for all areas of negative vorticity; then $\Gamma = \Gamma_+ + \Gamma_-$. For inviscid flows it can be proven that the three quantities in Eq. (3) are conserved. If the viscosity is nonzero these quantities decay in time, although at different rates.

By making Eq. (1) dimensionless in the usual way, the Reynolds number is introduced:

$$\mathrm{Re} = \frac{L_0 V_0}{\nu} = \frac{L_0^2/T_0}{\nu} = \frac{\Gamma_0}{\nu}, \tag{4}$$

where L_0, V_0, T_0 and Γ_0 are characteristic scales for length, velocity, time and circulation, respectively. In this paper these scales are set equal to 1, so that $\mathrm{Re} = 1/\nu$, and in what follows all quantities are given in these dimensionless units. This implies that a vortex with a translation velocity of 2, say, travels 2 length units in 1 time unit.

2.2. *A finite-difference method*

The simulations described in this paper are performed with a finite-difference method. The method is based on a code developed by Orlandi and Verzicco (Orlandi, 1990; Verzicco et al., 1995), which is adapted to allow for a great variety of initial vorticity distributions, to allow for different boundary conditions, to include background vorticity and/or topography if needed, and to have the possibility to follow the motion of passive tracers; not all of these features are used in this paper.

The finite-difference method used here applies a discretization of the equations on a rectangular grid in a rectangular domain in the x, y-plane. The time evolution in Eq. (1) is computed with an explicit third-order Runge–Kutta scheme, the viscous term with a Crank–Nicolson scheme, and the nonlinear term with the Arakawa scheme. The use of the Arakawa scheme (Arakawa, 1966) guarantees, on the one hand, that in the inviscid case energy, enstrophy and skew symmetry are conserved, and on the other hand, that the computation has a high degree of stability. The stability

is linked to the so-called Courant number CFL, which is a measure of the maximum velocity on the grid:

$$\mathrm{CFL} = \max\left\{\frac{|u|}{\Delta x} + \frac{|v|}{\Delta y}\right\}\Delta t, \tag{5}$$

with Δx and Δy the mesh size in the x- and y-direction, respectively, and Δt the time step. When only nonlinear terms are used, the numerical method is stable as long as $\mathrm{CFL} \leqslant \sqrt{3}$. If viscosity plays a role too, the stability becomes even better and CFL could be taken somewhat larger than $\sqrt{3}$. For the simulations presented in this paper CFL is kept below its limit (CFL is typically about 1.4 at $t=0$; it decreases in time as viscous effects reduce the velocities). The Poisson equation (2) is solved with a Fourier analysis and cyclic reduction (FACR) routine. This routine limits the choice in number of grid cells to 2^n ($n=1,2,3,\ldots$) in either direction, but the advantage is that it is a rather fast routine.

At the boundaries of the domain boundary conditions have to be applied. For the simulations of the dipolar vortices presented in this paper, periodic boundaries are used on all sides. In the x-direction, which is the direction of motion of the dipoles, this means that when the dipole leaves the domain on one side, it re-enters on the opposite side. Using periodic boundaries in the y-direction is equivalent to using free-slip walls as long as the dipole moves along the symmetry axis of the domain, which is the case throughout this paper.

2.3. Viscous decay of a Rankine vortex

To determine whether the numerical method handles viscous decay in a correct way, the simple case of a decaying Rankine vortex is used as a test case.

A Rankine vortex is a single-signed monopolar vortex with a rigid-body rotation in a circular region $r<a$, and outside this region the flow is irrotational:

$$\omega = \begin{cases} \omega_0, & r < a, \\ 0 & r > a, \end{cases} \tag{6}$$

where r is the radius with respect to the centre of the monopole. This vortex is a stable solution of the inviscid vorticity equation (Eq. (1) with $\nu=0$); see e.g. Dritschel (1988). The viscous decay of a Rankine vortex in an infinite domain has been studied analytically by Terazawa (1922), who found that the decay of the maximum of vorticity – once the decay has started this is located at the vortex centre – is described by

$$\omega_{\max}/\omega_0 = 1 - \exp(-a^2/4\nu t), \tag{7}$$

and the profile of vorticity at time t along an arbitrary radial line is described by a summation of an infinite series of first-order Bessel functions.

The numerical method requires a finite domain, yet a good comparison is possible if the boundaries are far enough away from the vortex. For the comparison, a Rankine vortex with radius $a=1$ and vorticity level $\omega_0=1$ is placed at the centre of a 10×10 domain. The number of grid cells is 128 in either direction, so that the grid spacing is $\Delta x=\Delta y\approx 0.078$. Fig. 1 shows radial vorticity profiles at the moments in time for which Terazawa (1922) gives analytical values: the difference between analytical and numerical values is less than 0.5%. The computed maximum of vorticity

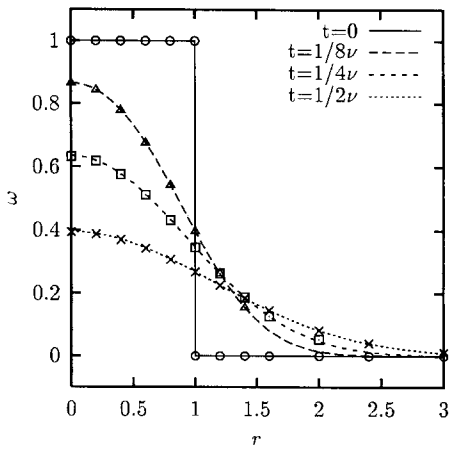

Fig. 1. Radial profiles of vorticity of a Rankine vortex which decays due to viscous effects. The solid line shows the initial vorticity distribution and the subsequent lines show the vorticity profiles at the moments in time for which Terazawa (1922) gives analytical values; these values are shown by symbols.

appears to given by Eq. (7), with differences also less than 0.5%. (The computation of Fig. 1 is done with $\mathrm{Re} = 1/\nu = 1000$, but the precise value is not important, since the decay time scales with $1/\nu$; differences between results obtained at different ν-values are less than 0.1%.)

The finite-difference method clearly handles viscous decay very well, even at a rather coarse grid, as long as ν is large enough (i.e. if $(\Delta x)^2 < \nu \Delta t$). From this example it is also clear that even though the initial Rankine vortex with its steep gradient in the vorticity is not well described by a grid method, possible imperfections in the initial vorticity distribution have no significant effect on the evolution of the vortex. Any gradient in the vorticity arising from such an imperfection would no doubt accelerate the decay of the vortex, especially if the resolution would be insufficient.

3. Theory of the Lamb dipole

Motions in a 2D inviscid infinite fluid are described by the vorticity equation (1) with $\nu = 0$, together with the Poisson equation (2). A steady inviscid flow solution must therefore satisfy:

$$J(\omega, \psi) = 0, \qquad \omega = -\nabla^2 \psi. \tag{8}$$

That $J(\omega, \psi) = 0$ implies that the vorticity of such a steady solution can be described by any function of the streamfunction: $\omega = F(\psi)$, where F must be an integrable function. One of the possible solutions is Eq. (6): the Rankine vortex.

Lamb (1932) constructed a dipolar solution with a continuous vorticity distribution inside a circular region by assuming a linear relationship between vorticity and streamfunction within this circle $r = a$, and outside the circle an irrotational motion:

$$\omega = \begin{cases} k^2 \psi, & r < a, \\ 0, & r > a, \end{cases} \tag{9}$$

with k some constant. The (potential) flow outside the circle is that of a cylinder placed in a uniform flow with a velocity $\boldsymbol{v}=(U_0,0)$ at infinity, which is given by

$$\psi(r,\theta)=-U_0\left(r-\frac{a^2}{r}\right)\sin\theta, \quad r\geqslant a, \tag{10a}$$

where r is the radial distance to the centre of the circle and θ the angle with respect to the flow direction. After matching the streamfunction and the velocities of the interior and exterior solutions at the edge of the circle $r=a$, the interior solution takes the following form:

$$\psi(r,\theta)=\frac{-2U_0}{kJ_0(ak)}J_1(kr)\sin\theta, \quad r\leqslant a, \tag{10b}$$

where J_n is the nth order Bessel function of the first kind, and ak the first zero of J_1:

$$J_1(ak)=0 \quad\longrightarrow\quad K_0\equiv ak\approx 3.8317, \tag{11}$$

with the constant K_0 introduced for clarity in the remainder of the paper. This stable solution is generally referred to as the Lamb dipole.

Seen in a fixed frame, the Lamb dipole moves along a straight line ($\theta=0$) with a constant velocity (U_0) and without change of form. The dipole consists of two oppositely signed vorticity halves which lie symmetrically about its line of motion. Inserting Eqs. (9), (10a) and (10b) in the definitions of circulation, energy and enstrophy given by Eq. (3) shows that these quantities can be expressed in terms of U_0 and a (Flór and Van Heijst, 1994; Nielsen and Juul Rasmussen, 1997):

$$\Gamma_+\approx 6.83U_0a, \quad E=2\pi U_0^2a^2, \quad H=\pi U_0^2K_0^2, \tag{12}$$

which are conserved in an inviscid infinite fluid. The intention of this paper is to investigate the effect of a finite domain and viscosity on the motion and shape of the Lamb dipole and on the value of the quantities in Eq. (12).

Recently, the work of Chaplygin on dipolar vortices has been rediscovered (see Meleshko and Van Heijst, 1994) and it appears that Chaplygin (1903) found a steady inviscid flow solution using a more general linear relation than Eq. (9) between vorticity and streamfunction inside a circle of radius a:

$$\omega=\begin{cases} k^2(\psi-\lambda), & r<a,\\ 0, & r>a, \end{cases} \tag{13}$$

where λ is some constant. The potential flow outside the circle is again given by Eq. (10a), while the vorticity in the interior is described by

$$\omega=\frac{-2U_0k}{J_0(ak)}J_1(kr)\sin\theta+\lambda k^2\frac{J_0(kr)}{J_0(ak)}, \quad r\leqslant a \tag{14}$$

where ak is given by Eq. (11). This solution is called the Chaplygin dipole. The Lamb dipole is clearly only a special case of the Chaplygin dipole, viz. with $\lambda=0$.

The Chaplygin dipole – which has zero total circulation for all λ – moves along a straight line ($\theta=0$) with a constant velocity (U_0) and without change of form. Both the Lamb dipole and the Chaplygin dipole have a vorticity distribution which is symmetric about a line through the extrema

of vorticity, and this symmetry line is perpendicular to the line of motion. Unlike for the Lamb dipole, however, the vorticity distribution of the Chaplygin dipole is *not* symmetric about the line of motion, the asymmetry being determined by the value of λ. The latter characteristic of the Chaplygin dipole makes a study of the effect of a finite domain and viscosity on the dipole's motion far more complicated and therefore merits a separate study. The reader is referred to Meleshko and Van Heijst (1994) for a discussion of the rediscovery of the Chaplygin dipole and some of its characteristics.

4. Simulation of the Lamb dipole

As mentioned in the preceeding section, the Lamb dipole moves in an infinite inviscid fluid with uniform velocity along a straight line and without change of form. In this section the effects of the finiteness of the domain and nonzero viscosity on the behaviour of the Lamb dipole and its characteristics are investigated numerically, using the finite-difference method outlined in Section 2.2.

The domain used for the computation measures 6×6 and is divided in 256×256 grid cells, so that $\Delta x=\Delta y\approx0.023$. The Reynolds number is $\mathrm{Re}=1/\nu=1000$. The Lamb dipole is initialized with a velocity $U_0=2$ in the positive x-direction and with a radius $a=1$, so that initially $k=K_0/a\approx3.8317$.

4.1. The Lamb dipole at $t=0$

When placed in a finite domain the Lamb dipole is affected by the boundaries of the domain. With (periodic) boundaries symmetrically on either side, parallel to the dipole axis, a flow in the direction opposite to the dipole's motion is induced and the dipole is slowed down: it moves with a velocity $U<U_0$. The dipole is slowed down by the effect of the image dipoles in the image domains on either side of the computational domain. And the narrower the domain is, the lower is the dipole's velocity U at a given U_0. Since the flow configuration is symmetric about the dipole's axis, the x-axis, the dipole continues to move along this axis, no matter what shape deformations may occur.

In the frame co-moving with the dipole the relation between vorticity and streamfunction is a linear one, given by Eq. (9): $\omega/\psi=k^2$. The velocity of the co-moving frame with respect to the nonmoving frame, i.e. the dipole's velocity U, is found by minimizing the "scatter" around this line in an ω,ψ-plot. In minimizing the scatter, only absolute vorticity levels larger than 0.1 times the vorticity maximum $\omega_{\max}$ are used. This is done to omit the region of low-value vorticity where later in the evolution nonlinearities occur (see for instance Fig. 3). The range from 0.1 to 1 times $\omega_{\max}$ is divided in 10 vorticity bands and in each band the scatter – the horizontal spread $\Delta\psi$ in the ω,ψ-points – is averaged. Minimum scatter is reached when the sum of these averages is minimal. Table 1 lists dipole velocities for a number of domain widths. For the 6×6 domain used in this paper the initial velocity of the dipole appears to be $U=1.825$. In the co-moving frame the streamline $\psi=0$ defines the circular edge of the dipole. Numerically, it is found in this way that the dipole's radius is $a=0.999$.

4.2. The Lamb dipole at $t=100$

Fig. 2 shows contours of vorticity of the evolved dipole at time $t=100$; the dipole has then moved 17 times through the whole domain in the x-direction. The ±0.1 contour shows that the

Table 1
The initial velocity U of a Lamb dipole initialized with $U_0 = 2$ and $a = 1$, centred in a domain with periodic boundaries at $y = \pm y_w$

y_w	2.0	3.0	4.0	5.0	6.0	7.0	8.0	9.0	10.0
N	128	128	128	256	256	256	512	512	512
U	1.591	1.825	1.906	1.940	1.960	1.970	1.977	1.988	1.987

Note: The number of grid cells N is varied along with the width of the domain to keep the mesh size more or less the same. The computations presented in Sections 4 and 5 are done with $y_w = 3$ and $N = 256$.

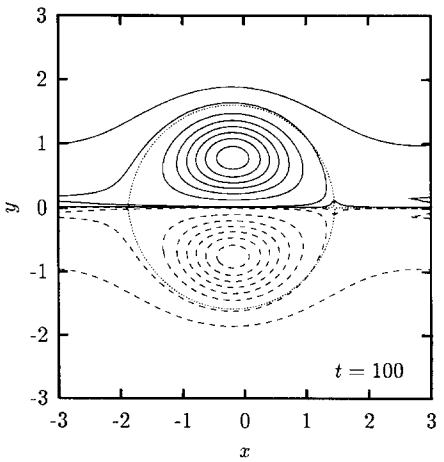

Fig. 2. Contours of vorticity of the evolved Lamb dipole at time $t = 100$. Contours are drawn at ± 0.01, ± 0.1, ± 1, ± 2, ± 3, ± 4, ± 5 and ± 6; positive is solid, negative is dashed. The dotted line is the streamline $\psi = 0$ in the frame co-moving with the dipole, which marks the edge of the dipole. (At $t = 0$ the line $\psi = 0$ is a circle of radius 1.)

dipole leaves a "tail" of low-value vorticity behind as it moves. That such a tail is formed is inherent to the grid method, since for the value of the vorticity at grid point i, j at time $t + \Delta t$ the value of the vorticity at time t in all 8 grid points around i, j is needed. This "extra" vorticity is low-level vorticity and it dies out due to viscous effects, so the influence it has on the dipole's motion is minimal[1], and largest at the beginning of the computation when the vorticity distribution has to "adapt" itself to the boundary conditions. The extra vorticity shows up as a small increase in the total circulation and as a small dip in the dipole's velocity after the first cycle when it reaches its own tail (at about $t = 4$ in this case). The ± 0.01 contour encloses an area of lower-level vorticity generated in previous cycles as the dipole interacts with its own tail.

The dotted line in Fig. 2 is the streamline $\psi = 0$: the edge of the dipole. It can be seen clearly that the size of the dipole has increased. Along a line through the extrema of vorticity the radius is $a = 1.586$. The increase in size is a consequence of viscous effects, which spread the vorticity over a larger area. At the same time the extrema of vorticity decrease: in Fig. 2 their values

[1] Like the dipole itself, the extra vorticity is symmetrically arranged with respect to the dipole axis, hence it does not cause the dipole to move away from its initial line of motion.

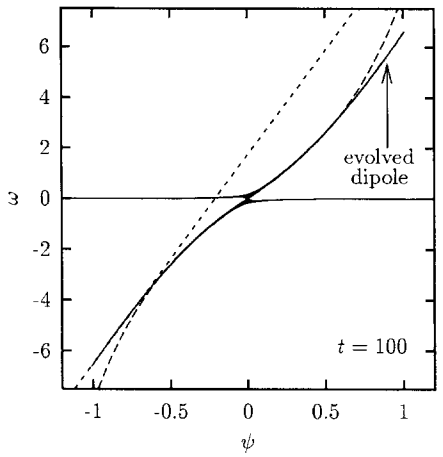

Fig. 3. The relation between vorticity ω and streamfunction ψ of the full domain with the evolved dipole at time $t = 100$ is given by the curve (the two dipole halves) and the more or less horizontal line at low vorticity values (the area outside the dipole halves). The central part of the graph shows the values at the edge of the dipole and at its axis. The two dashed lines are discussed in the text.

are ± 6.610, whereas initially their values were ± 22.127. The edge of the dipole is not a perfect circle: at the rear side it is a little stretched with respect to a circle, but only some 2%, hence, the evolving dipole remains fairly circular throughout its evolution.

The line $\psi = 0$ in Fig. 2 follows from the streamfunction in the frame moving along with the dipole. The velocity of the dipole is found by minimizing the "scatter" in the ω, ψ-plot shown in Fig. 3. The relation between vorticity and streamfunction at $t = 100$ is no longer linear, both in the branches of the two dipole halves (the two curved lines) and around the edge of the dipole. The latter is in Fig. 3 the region of small vorticity values at the centre of the graph; also the tail of the dipole gives a contribution in that region. This region is therefore omitted from the graph when minimizing the scatter around the ω, ψ-curve to find the dipole's velocity, as outlined in Section 4.1. For the dipole of Fig. 2, a velocity $U = 0.606$ is found, which is the dipole's velocity in the nonmoving frame at $t = 100$.

It has been shown theoretically, numerically and experimentally (see e.g. Joyce and Montgomery, 1973; Montgomery et al., 1992; Pasmanter, 1993; Flór and Van Heijst, 1994) that under certain conditions the steady-state structures which emerge from 2D flows show a relationship between vorticity and streamfunction of the form $\omega \propto \sinh(A\psi)$. The long-dashed line in Fig. 3 is the function $\omega = 2.2 \sinh(2\psi)$. This curve fits the nonlinear part of the ω, ψ-relation reasonably well. The numerical factor in front of the sinh depends on time: it decreases with time (at $t = 50$, for instance, it is 3.1). With the value $A = 2.0$ the $\sinh(A\psi)$-function fits the curve best: with $A = 1.9$ the curvature is too weak, and with $A = 2.1$ the curvature is too strong. At this stage in the evolution, there is no $\sinh(2\psi)$-function that covers the entire ω, ψ-relation: the dipole is still linear at the extrema of vorticity.

The linear part of the ω, ψ-relation at the vorticity minimum is indicated by the short-dashed line in Fig. 3 (a similar line can be drawn at the vorticity maximum). The angle of this line shows that $\omega \propto (2.869)^2 \psi$ at the vorticity extrema. Hence, the value of k in the part of the dipole

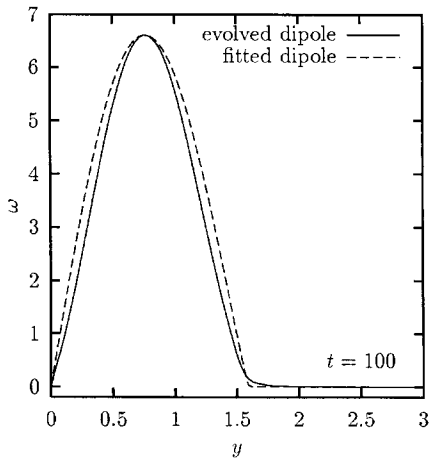

Fig. 4. Profile of vorticity along a line through the extrema of vorticity of the evolved dipole (solid line) at time $t = 100$, compared with the profile of an initial Lamb dipole (dashed line) fitted to the radius and the maximum of vorticity of the evolved dipole. For clarity only the positive half of the dipoles is shown; the negative half looks the same, but is mirrored in the origin.

that is still linear is $k = 2.869$, showing that k has decreased with time (at $t = 0$, k was equal to $K_0 \approx 3.832$). Assuming that in this linear part relation (11) is still valid, the radius of the dipole is $a_{\text{lin}} = K_0/k \approx 1.336$, which is larger than the initial value $a = 1$. Combining the value of k with the radius a found from the $\psi = 0$ streamline above shows that ak is well above 4 (with $a = 1.586$, $ak = 4.551$). The latter result is of course no more than qualitative, since k is determined from the linear part of the dipole only, whereas a follows from the entire dipole. Yet, it shows that as the dipole evolves both a and ak increase and k decreases.

These results are different from results reported by Swaters (1991), who assumes that ak is constant in time and then finds that a is constant in time, so that also k is constant in time. The origin of the difference in results lies in the fact that Swaters uses Rayleigh damping (like the damping due to an Ekman layer at the bottom of a rotating tank, in experimental terms) rather than horizontal diffusion, as can be seen from Swaters' vorticity equation:

$$\frac{\partial \omega}{\partial t} + J(\omega, \psi) = \frac{1}{R}\omega, \tag{15}$$

where R is the Rayleigh number. According to this model, there is no mechanism to spread vorticity over a larger area, hence it is no surprise that the dipole radius remains the same throughout the dipole's evolution.

Since the ω, ψ-relation of the evolved dipole is not linear, this dipole is no longer a Lamb dipole. Yet, it is still "Lamb-like", meaning that it still resembles a Lamb dipole fairly closely. A straight line $\omega = k_{\text{ext}}^2 \psi$ connecting the extrema of the ω, ψ-relation (Fig. 3), for instance, results in a value of $k_{\text{ext}} = 2.559$, only about 10% less than the k-value found from the linear parts of the ω, ψ-relation ($k = 2.869$).

That the evolved dipole is still Lamb-like can also be seen from a cross-section of the vorticity profile along a line through the vorticity extrema. The solid line in Fig. 4 shows the profile of the

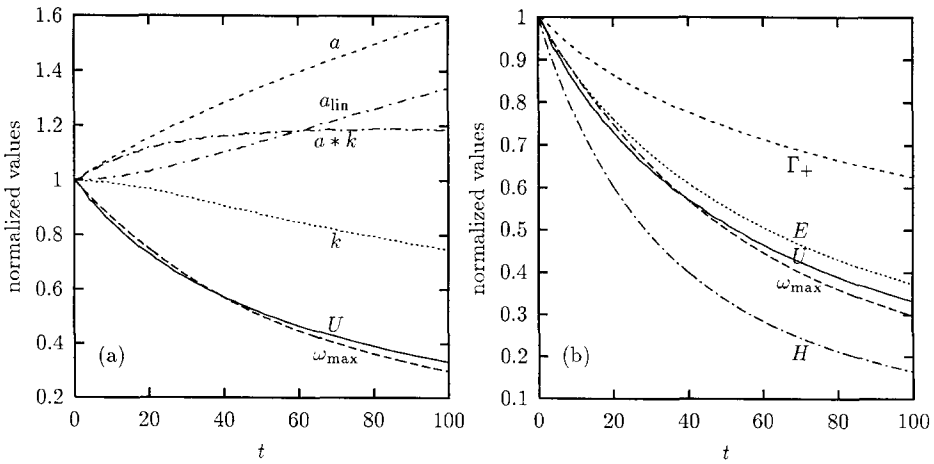

Fig. 5. Some quantities of the evolving Lamb dipole as a function of time, normalized to unity at $t = 0$. For clarity not all quantities are put in a single graph; both (a) and (b) show the maximum of vorticity (ω_{max}) and the velocity (U) of the dipole for comparison. The absolute value of the vorticity minimum ($|\omega_{min}|$) always equals ω_{max}. See the text for details on the quantities given by the other lines. Absolute values of all quantities at three moments in time are given in Table 2.

evolved dipole. This dipole has a radius $a = 1.586$ and a maximum of vorticity of 6.610. These values can be used to determine the characteristics of an initial Lamb dipole that "fits" the evolved dipole by adapting the parameter U_0 in Eq. (10b). The profile of this "fitted" Lamb dipole is shown in Fig. 4 by a dashed line: the resemblance between the two lines is rather good. All in all, the evolved dipole still has many characteristics similar to those of an initial Lamb dipole: the evolved dipole is Lamb-like.

In their laboratory experiments Flór and Van Heijst (1994) found also that the profile of an evolved dipole matches that of a Lamb dipole quite well, and the profile of their evolved dipole "peaks" somewhat more in the vorticity extrema than the profile of a Lamb dipole, as is the case in Fig. 4. Unlike the experimental results, though, the evolved dipole of Fig. 4 shows no oppositely signed vorticity outside the vortex, indicating that it is an experimental feature.

4.3. The evolution of the Lamb dipole

Fig. 5 shows some quantities of the evolving Lamb dipole as a function of time between $t = 0$ and 100; the quantities are normalized by their initial values to ease a comparison between the rates of increase and decrease. Absolute values of these quantities are listed in Table 2 for three moments in time. It is not possible to fit any of the decaying quantities with an exponential function: the best least-square exponential fit is a curve which decreases slower at the beginning of the evolution than the computed values do, and faster later on.

The velocity of the dipole, U, is determined by minimizing the scatter in the ω, ψ-relation in the co-moving frame, as outlined in Section 4.1. In this co-moving frame the ω, ψ-relation has a linear part near the extrema of vorticity – as in Fig. 3 – and this linear part determines the value of k, which decreases in time. As the vorticity is spread over a larger area, the radius a of the dipole

Table 2
Absolute values at three moments in time of the quantities of the evolving Lamb dipole plotted in Fig. 5

Quantity	$t=0$	$t=50$	$t=100$
ω_{max}	22.127	11.129	6.610
U	1.825	0.939	0.606
a	0.999	1.338	1.586
k	3.833	3.351	2.869
ak	3.830	4.483	4.551
a_{lin}	1.000	1.144	1.336
Γ_+	13.658	10.152	8.530
E	24.043	13.323	8.978
H	184.499	61.994	30.412

increases; see Fig. 5a. This radius is the point where the streamfunction ψ equals zero (in the co-moving frame) along a line through the extrema of vorticity. The product $a\,k$, also shown in Fig. 5a, increases in time to a more or less constant value of about 4.54. As mentioned in Section 4.2 this is only a qualitative result since k is determined from the linear part of the dipole only, whereas a follows from the entire dipole. Assuming that for the linear part of the ω,ψ-relation Eq. (11) remains valid, a radius for this linear part $a_{lin}=K_0/k$ can be computed. This quantity increases in time too, but not as fast as the real radius of the dipole, as Fig. 5a shows.

Nielsen and Juul Rasmussen (1997) derived for the decaying Lamb dipole the time dependence of the velocity and the radius:

$$U(t)=\frac{U(0)a^2(0)}{\nu K_0^2 t+a^2(0)}, \tag{16a}$$

$$a(t)=\sqrt{\nu K_0^2 t+a^2(0)}, \tag{16b}$$

and they find that these functions describe their results quite well (their simulations are done with a spectral method and are terminated at about $t=45$ in units of the present paper). Fig. 6 shows that the increase of the radius of the Lamb dipole of Fig. 5 is reasonably well described by Eq. (16b), but the velocity decreases considerably faster than is predicted by Eq. (16a). The origin of this discrepancy between Eq. (16) and the numerical results is not clear.

The decay of the vorticity is determined by viscosity. Assuming that $\omega=k^2\psi$ is valid throughout the evolution of the dipole, the purely viscous decay of the vorticity – which follows from the vorticity equation (1) – is given by

$$\frac{\partial\omega}{\partial t}=\frac{\nabla^2\omega}{\mathrm{Re}}=-\frac{k^2\omega}{\mathrm{Re}}. \tag{17}$$

The solution of this differential equation is

$$\omega(t)=\omega(t=0)\exp(-k^2t/\mathrm{Re}). \tag{18}$$

With $\mathrm{Re}=1/\nu=1000$ and $k=K_0$ (from Eq. (11) with radius $a=1$) in this equation, the maximum of vorticity decreases faster than the vorticity from the computations does. At $t=100$, for instance,

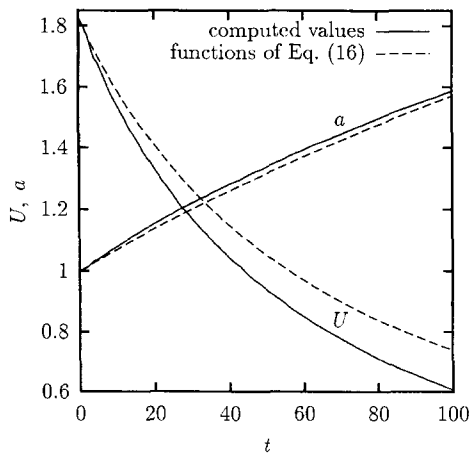

Fig. 6. Velocity U and radius a of the evolving Lamb dipole of Fig. 5 compared with the functions given by Eq. (16), using the initial values given in Table 2 for $U(0)$ and $a(0)$. Both U and a are shown in absolute values in this graph.

the computed maximum of vorticity is 6.610 and the value using Eq. (18) is 5.097. Fig. 5a shows that k actually is a function of time. Using the $k(t)$ found from the computations in Eq. (18) results in a vorticity maximum that decreases slower than the computed vorticity (at $t = 100$ the value is 9.716). Since both the velocity and the radius of the dipole change in time, what effectively happens is that the Reynolds number Re, defined by Eq. (4), also depends on time (cf. Nielsen and Juul Rasmussen, 1997):

$$\mathrm{Re}(t) = \frac{a(t)U(t)}{va(0)U(0)}. \tag{19}$$

Using the values from the computation for $k(t)$ and $\mathrm{Re}(t)$ in Eq. (18) gives a decrease of the maximum of vorticity which is even faster than the decrease is for constant Re and $k = K_0$ in Eq. (18).

Neither of these attempts are very successful in describing the decay of the maximum of vorticity nor the decay of the vorticity is clearly not as fast as expected from simple scaling arguments. This indicates that as soon as the ω,ψ-relation is no longer linear, the decay of the vorticity is not well described by the above model. (This decay cannot be affected much by "numerical viscosity", since the decay of the Rankine vortex, discussed in Section 2.3, is described quite well with the numerical model.) If the Lamb dipole is placed in an infinite fluid without viscosity, it moves along a straight line with constant velocity and without change of form, and the ω,ψ-relation remains linear, as mentioned in Section 3. The dipole's motion is solely due to the nonlinear effects in that case. Adding viscosity means that vorticity is spread over a larger area and apparently the ω,ψ-relation then becomes somewhat nonlinear, so that also nonlinear effects participate in changing the form of the dipole and the ω,ψ-relation. Since the boundaries of the domain affect the velocity of the dipole (see Table 1), these boundaries no doubt also affect the shape of the dipole and the ω,ψ-relation via the nonlinear advection effects.

Fig. 5b shows the decay of three quantities integrated over the whole domain: the positive circulation Γ_+ (the circulation of all areas of positive vorticity), the energy E and the enstrophy H;

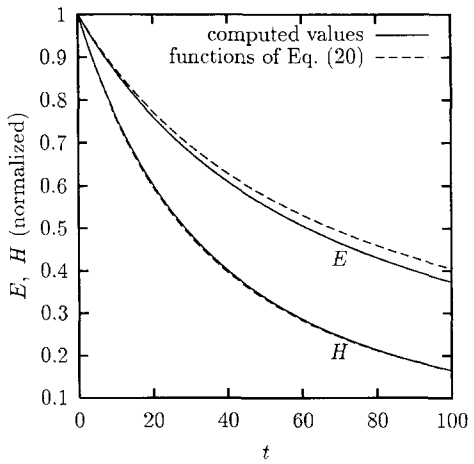

Fig. 7. Decay of energy E and enstrophy H in time as in Fig. 5, compared with the functions given by Eq. (20), using the initial values given in Table 2 for $U(0)$ and $a(0)$. All curves are normalized to unity at $t=0$.

their definitions are given in Eq. (3). The positive circulation does not decrease as fast as the maximum of vorticity does: viscosity spreads the vorticity faster over a larger area – thus decreasing the extrema – than that it decreases vorticity in the domain as a whole. Nielsen and Juul Rasmussen (1997) derive from Eq. (12) for the decaying Lamb dipole the time dependence of the energy and the enstrophy:

$$E(t)=\frac{2\pi a^2(0)U_0^2}{\nu K_0^2 t/a^2(0)+1}, \tag{20a}$$

$$H(t)=\frac{\pi K_0^2/U^2(0)}{(\nu K_0^2 t/a^2(0)+1)^2}, \tag{20b}$$

and they find that these functions describe their results quite well. Fig. 7 shows that this is also the case for the dipole described here, especially for the enstrophy.

In the computations described here there are 256 grid cells in either direction. Using 128 grid cells gives basically the same results, although there are somewhat larger fluctuations on the curves of Fig. 5, especially at the beginning of the computation (until about $t=10$), when the initial vorticity distribution has to "adapt" itself to the boundary condition. Decreasing the number of grid cells further makes these differences and fluctuations larger, also because the resolution of small-scale effects becomes worse. Similarly, increasing the number of grid cells reduces the small fluctuations visible in Fig. 5 but this does not alter the overall results.

4.4. *The fate of the decaying Lamb dipole*

If the computation continues after $t=100$ the same trend continues: the radius increases, the extrema of vorticity decrease, the velocity decreases, etc. Eventually, viscosity has spread the vorticity over the entire domain and a clear dipolar structure is no longer defined. The dipole's ω,ψ-relation

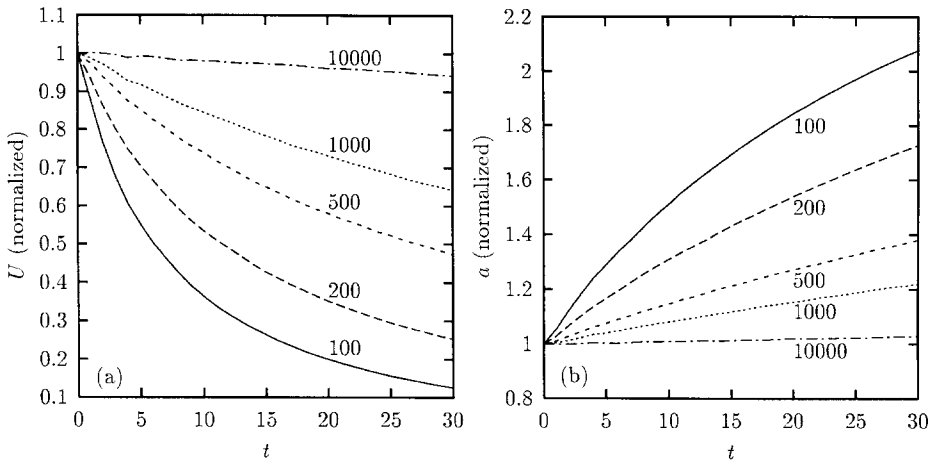

Fig. 8. (a) Velocity U and (b) radius a of the evolving Lamb dipole as a function of time, both normalized to unity at $t = 0$, for five different Reynolds numbers Re: 100, 200, 500, 1000 and 10 000. (The Re = 1000 case is given in Fig. 5 until $t = 100$.)

then no longer has a linear part near the vorticity extrema, as is still the case in Fig. 3, and it can be described entirely by $\omega = C \sinh(2\psi)$, with C depending only on time.

Continuing the computations until that stage is hardly useful since (long) before that the dipole has become so big that the effects of the boundaries become significant. At $t = 100$ the dipole has a diameter of about 3.2, whereas the domain has a width of 6 (see Fig. 2), so that the size of the dipole is roughly the same as the distance between the edges of the dipole and of its periodic images in the domains on either side of the computational domain.

4.5. *The effect of the magnitude of the Reynolds number*

Using a Reynolds number Re larger than the Re = 1000 used for the above computations means that the viscous decay is less strong, so that the dipole's radius grows slower and the extrema of vorticity decrease slower, and hence the dipole's velocity decreases slower. This implies that the dipole remains Lamb-like for a longer time.

Vice versa, for larger viscosity values the dipole grows faster and its velocity decreases faster. And the tail of vorticity left behind by the dipole becomes more and more pronounced as viscosity increases. How long the evolving dipole retains its Lamb-like characteristics depends on the magnitude of the viscous effects: the smaller the Reynolds number is, the sooner the dipole has lost its Lamb-like characteristics.

Fig. 8 shows the relative change in the velocity U and the radius a of the evolving Lamb dipole for five values of the Reynolds number until $t = 30$. The computations are stopped at that moment since the radius of the dipole in the Re = 100 case is then more than 2: the dipole has become so large that the front of the dipole is within its own tail, and the $\psi = 0$ line is no longer a closed line around the dipole, as is the case in Fig. 2 (which is for Re = 1000 at $t = 100$). The ω, ψ-relation of this dipole still shows a more or less linear part near the vorticity extrema, but that part is quite small. In fact, the ω, ψ-relation can be described very well, including the extrema of vorticity, by

the function $\omega = 1.34 \sinh(2\psi)$: the dipole has become entirely nonlinear (the scatter around this curve is bigger than the scatter in Fig. 3, but the relation is quite clear).

The $\psi = 0$ line for $\mathrm{Re} = 200$ is at $t = 30$ still fairly circular: it is stretched at the rear side only about 5% with respect to a circle. The tail of low-value vorticity of the $\mathrm{Re} = 200$ dipole is at $t = 30$ somewhat more pronounced than the tail in Fig. 2, and dipole's velocity (0.461) is smaller and its radius (1.725) is larger than those of the dipole in Fig. 2. The ω, ψ-relation clearly shows a linear part at the extrema of vorticity, like in Fig. 3 [the nonlinear part is described well by $\omega = 1.92 \sinh(2\psi)$]. In other words, the evolved dipole in the $\mathrm{Re} = 200$ case is at $t = 30$ still Lamb-like, whereas the evolved dipole in the $\mathrm{Re} = 100$ case has lost most of its Lamb-like characteristics.

The finite-difference method used here allows for inviscid computations and a run done without viscosity shows that the Lamb dipole moves, indeed, with constant velocity, constant vorticity extrema and constant radius: all quantities fluctuate within 0.5% around their average for $t = 0$ to $t = 30$, except for a very small decay of the order of $10^{-5} t$, which may be attributed to "numerical viscosity". This result shows that the decay of the Lamb dipole described above is caused by viscous rather than numerical effects.

5. Other symmetrical dipolar vortices

As discussed above, the Lamb dipole placed in a finite domain with a viscous fluid remains Lamb-like for a long time, which shows that the Lamb-like structure is a very stable one. Do other dipolar vortices that are no solution of the inviscid vorticity equation but which have symmetry properties like the Lamb dipole (and thus initially have a net linear momentum) assume Lamb-like characteristics? Or, in other words: do such vortices evolve to a Lamb-like dipole? To address this question three examples of other dipolar vortex structures are discussed below[2]. The Reynolds number is $\mathrm{Re} = 1000$ and the domain and grid size are as in Section 4.

5.1. Circular dipole with uniform vorticity patches

The first alternative dipole is circular and has two halves of oppositely signed uniform vorticity:

$$\omega = \begin{cases} \omega_0, & r < a, \ y > 0, \\ -\omega_0, & r < a, \ y < 0, \\ 0, & r > a. \end{cases} \tag{21}$$

Due to its dipolar vorticity distribution this vortex moves in the positive x-direction, like the Lamb dipole of the previous section.

Fig. 9 shows the vorticity distribution and the ω, ψ-relation of the initial vortex using $\omega_0 = 10$ and $a = 1$, and of the evolved vortex at $t = 4$ and 8 (the moments in time when the dipole has moved through the whole domain a little more than once and twice, respectively). As the dipole moves it leaves behind a tail of vorticity as discussed before for the Lamb dipole, but here the tail is more pronounced and it has a larger vorticity level. The reason for this is that a step-wise

[2] A recent numerical study by Nielsen and Juul Rasmussen (1997) shows that a Lamb-like dipole also emerges from a laminar jet of vorticity and from a turbulent patch of vorticity, both having a net linear momentum at initialization.

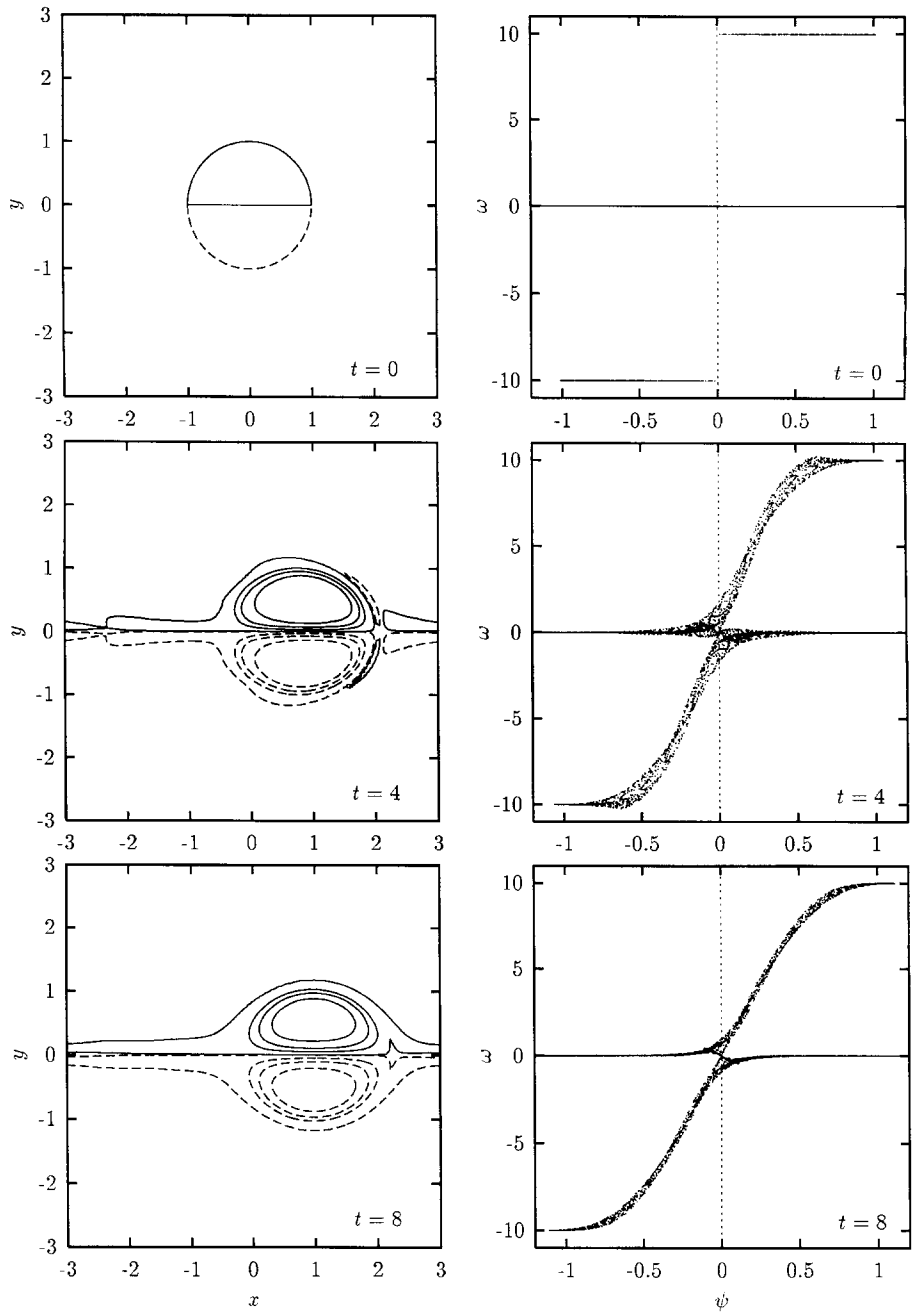

Fig. 9. Contours of vorticity (left) and ω,ψ-relations (right) of the initial dipole (top) given by Eq. (21) with $\omega_0 = 10$ and $a = 1$, and of the evolved dipole at $t = 4$ (middle) and $t = 8$ (bottom). In the left column vorticity contours are drawn at ± 0.1, ± 3, ± 6 and ± 9; positive is solid, negative is dashed. The dotted lines in the right column indicate $\psi = 0$.

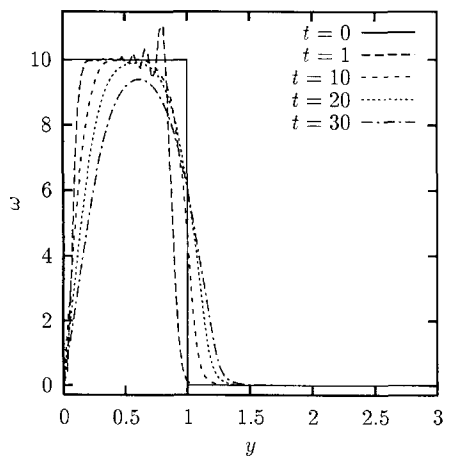

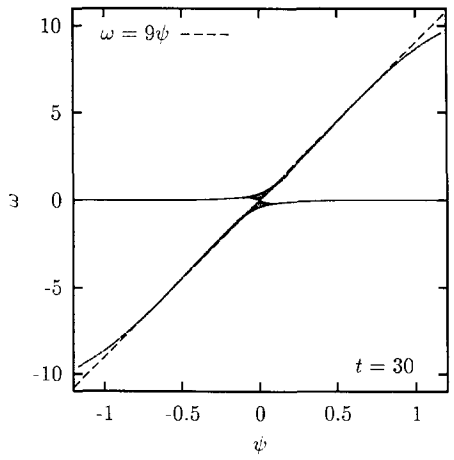

Fig. 10. Profiles of vorticity along a line through the extrema of vorticity of the initial ($t=0$; solid line) dipole given by Eq. (21) and of the evolved dipole at $t=1$, 10, 20 and 30. For clarity only the positive half of the dipoles is shown; the negative half looks the same, but is mirrored in the origin.

Fig. 11. Relation between vorticity and streamfunction of the evolved dipole initially given by Eq. (21) with $\omega_0=10$ and $a=1$, at $t=30$. The dashed line is the function $\omega=9\psi$.

vorticity function as in Eq. (21) is poorly represented by a grid method and there are relatively large fluctuations in the vorticity on top of the vortex and in its wake. As the middle row of Fig. 9 shows, some oppositely signed vorticity is also created at the front of the moving dipole. This "extra" vorticity lies symmetrically about dipole's line of motion, so the dipole continues to move along the same straight line.

The fluctuations on top of the vortex can also be seen in the profiles of vorticity shown in Fig. 10. At $t=1$ there are clearly large spiked fluctuations in the vorticity. As time evolves, viscosity smears out these fluctuations and the sharp edges of the vorticity distribution are smoothed quite quickly. At $t=10$ the vorticity profile is more or less flat again at the top of the vortex, but it has round edges. Later on the vorticity distribution becomes more and more smoothed, with at $t=30$ a profile very similar to that of a Lamb dipole.

Fig. 11 shows the ω,ψ-relation of the evolved dipole at $t=30$, which is an almost straight line for most of the dipole: only at the centres of the dipole halves the relation is not yet linear. As time goes on, these small nonlinearities disappear too and the entire ω,ψ-relation becomes linear: the dipole initially given by Eq. (21) has become a Lamb dipole. After that the decay described in Section 4 sets in and the ω,ψ-relation becomes nonlinear again, but now with tips pointing the other way, as in Fig. 3.

Determining the velocity of the evolving dipole by minimizing the scatter in the ω,ψ-plots (as done in Section 4) is at the beginning of the evolution not very reliable but it appears that the initial velocity is about 1.83, after which the velocity decreases. The velocity of this particular dipole is comparable with the velocity of the Lamb dipole described in Section 4. The reason for this is the (arbitrary) choice of the value of ω_0: with $\omega_0=10$ the initial circulation, energy and enstrophy appear to be of the same order as those of a Lamb dipole with $U_0=2$ at $t=0$.

Had the evolution started with a different ω_0-value, then the dipole's velocity would have been different, since for lower ω_0 the dipole has a lower velocity. The overall picture would be the same, though: after some time the dipole initially given by Eq. (21) has evolved into a Lamb dipole due to viscous and nonlinear effects, which is followed by the usual decay of the Lamb dipole. The time scale at which dipole Eq. (21) becomes a Lamb dipole depends not on ω_0, it appears from simulations, but on the magnitude of the viscous effects: the larger viscosity is, the faster a Lamb-like dipole is formed.

5.2. *Dipole consisting of two elliptic uniform monopoles*

Another initial case consists of a set of two ellipses of oppositely signed uniform vorticity:

$$\omega = \begin{cases} \omega_0, & \dfrac{(x-x_0)^2}{a^2} + \dfrac{(y-d)^2}{b^2} < 1, \\ -\omega_0, & \dfrac{(x-x_0)^2}{a^2} + \dfrac{(y+d)^2}{b^2} < 1, \\ 0, & \text{elsewhere}, \end{cases} \tag{22}$$

where (x_0, d) and $(x_0, -d)$ are the centres of the two ellipses and a and b the axes, with $d > 0$ and $a > b$. Single elliptic monopolar vortices with uniform vorticity (Kirchhoff vortices) are unstable if their aspect ratio (a/b) is larger than 3. In this study $a = 2b$ is used. In view of the size of the domain, $a = 1$ is a good choice. Since the ellipses are meant not to overlap each other, d should be larger than b. To avoid large influences of the upper and lower boundaries, the value of d should not be too large.

The dipole of Eq. (22) appears to evolve into a Lamb-like dipole, just like the dipole of Eq. (21) does. In this case, however, viscosity and nonlinear effects also have to mould the two ellipses into semicircles. If the two ellipses are right next to each other $(d = b)$ the formation of a Lamb-like dipole takes somewhat more time than is the case for dipole, Eq. (21). And the larger d is, the more time the process takes. Again, the value of ω_0 is not so important for the timescale of the formation of a Lamb-like dipole (this is mainly determined by the Reynolds number), but it is more important here than for dipole Eq. (21) since nonlinear effects are more important here.

As an example, consider the ellipses of Eq. (22) with $d = 0.7$, $a = 2b = 1$ and $\omega_0 = 10$. Fig. 12 shows contours of vorticity at some early stages in the evolution. Since a grid method represents a step function as in Eq. (22) poorly, fluctuations in the vorticity on the vorticity patches and in their wake arise – as discussed in relation to dipole Eq. (21). The initial form of the two patches is an ellipse, but their form changes immediately as they move closer together. At the same time viscosity smooths the sharp edges of the step function. At $t = 2.5$ the two patches have come close together and can be considered as one single vortex structure. There is still some oppositely signed vorticity at the front of the dipole halves. This vorticity is created initially by grid effects in the wake of the vortex and transported forward in between the two patches, as can be seen in the middle row of Fig. 12. When this vorticity arrives at the front of the patches, it is pulled outward and then transported along side to the back of the vortex again.

The velocity of the dipolar structure can be determined by minimizing the scatter in the ω, ψ-relation. Although early in the evolution this procedure is not very reliable, it gives a good idea of the velocity. At $t = 0.5$ (top-right in Fig. 12) the velocity is about 1.48, and at $t = 1$ it is about 1.44.

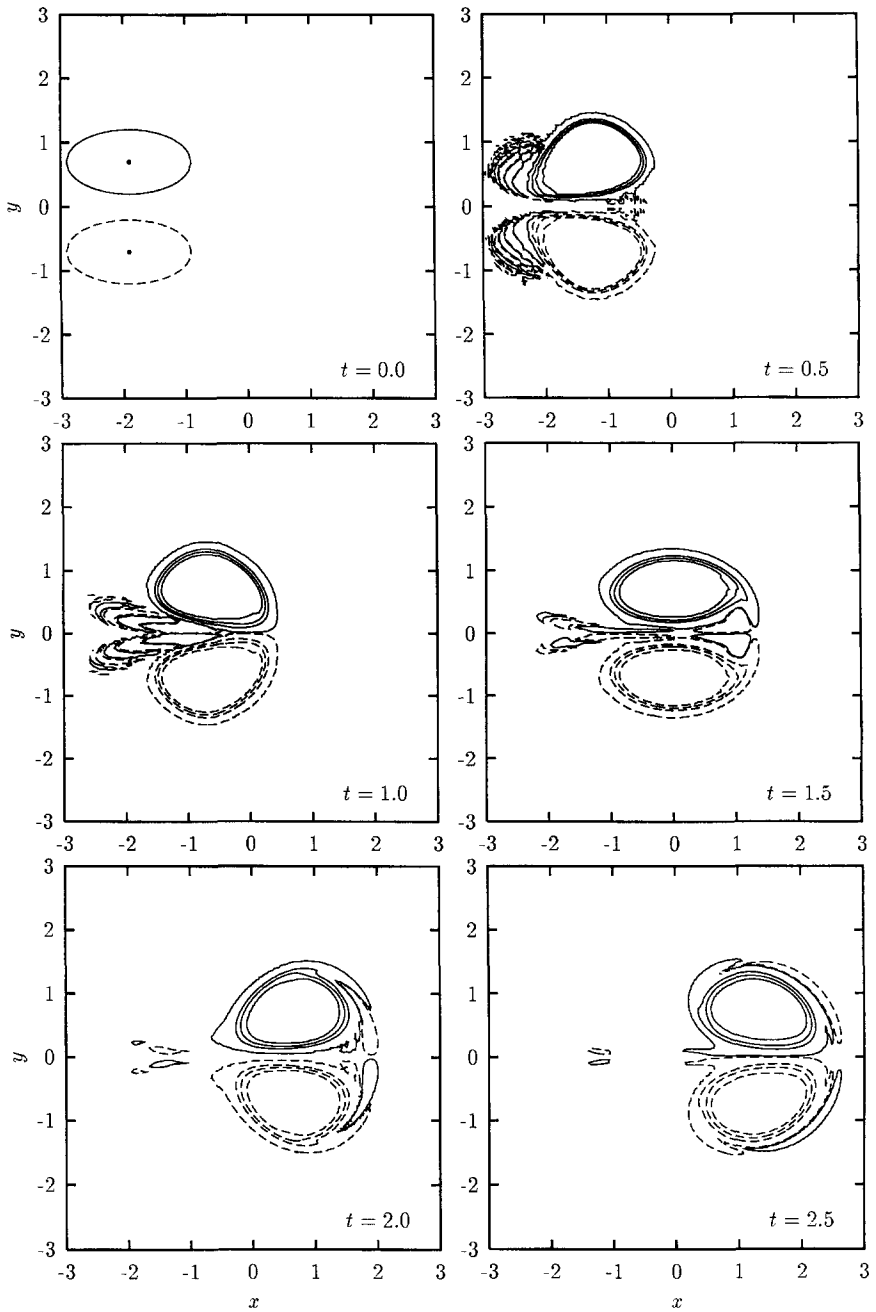

Fig. 12. Contours of vorticity at some early stages in the evolution of a dipole initially given by Eq. (22) with $\omega_0 = 10$, $a = 2b = 1$ and $d = 0.7$. In the top left plot ($t = 0$) two dots indicate the centres of the initial ellipses. Contours of vorticity are drawn at ± 0.1, ± 3, ± 6 and ± 9; positive is solid, negative is dashed.

Then the velocity decreases sharply to about 1.30 at 2 and for some time it remains almost constant. Between $t=2.5$ and $t=12$ the velocity (which can then be determined reasonably well) oscillates as it slowly decreases. Until $t=12$, apparently, there are oscillations in the form of the two patches while a single dipolar vortex is being formed. After $t=12$ the velocity simply decreases due to viscous effects: the main shape of the dipole is formed and it can assume Lamb-like characteristics. Its ω,ψ-relation at $t=30$ still shows clear nonlinearities throughout the entire dipole (more clear than in Fig. 11), but as time evolves further these nonlinearities disappear and a true Lamb-like dipole is formed, which subsequently decays as in the cases discussed before.

5.3. Dipole consisting of two elliptic Bessel-type monopoles

As a third example a dipole is constructed of two elliptic monopoles as in Section 5.2, but then with monopoles which have an initial vorticity distribution like that of a Bessel-type monopole.

The circular "Bessel monopole" is a steady solution of the inviscid vorticity Eq. (8) assuming a linear relation between vorticity and streamfunction as in Eq. (9):

$$\omega = \begin{cases} k_m^2\psi, & r<a, \\ 0, & r>a \end{cases} \tag{23}$$

and choosing for a monopolar solution. The streamfunction of this solution is given by

$$\psi = \begin{cases} \dfrac{\Gamma}{2\pi k_m a J_1(ak_m)} J_0(k_m r), & r\leqslant a, \\ \dfrac{-\Gamma}{2\pi}\log(r/a), & r\geqslant a, \end{cases} \tag{24}$$

where Γ is the total circulation of the monopole. The first nonzero root of J_0 determines the constant k_m:

$$J_0(ak_m)=0 \quad\longrightarrow\quad ak_m \approx 2.4048. \tag{25}$$

The Bessel monopole has single-signed vorticity with zero vorticity at the edge.

To form an elliptic Bessel-type monopole, an "equivalent radius" $\bar{a}$ for using in Eq. (24) is defined as

$$\bar{a} \equiv \frac{2ab}{a+b}, \tag{26}$$

where a and b are the axes of the ellipse, as in Eq. (22). This radius is formed like the relation between radius, surface and circumference of a circle, where the circumference of the ellipse is approximated by $\pi(a+b)$. The radial distance r_θ with respect to the centre of the ellipse in Eq. (24) is then given by

$$r_\theta^2 = \frac{a^2b^2}{a^2+(b^2-a^2)\sin\theta}, \tag{27}$$

where θ is the angle with respect to the positive x-axis. This elliptic Bessel monopole is not a solution of the inviscid vorticity equation.

Initially, two of these Bessel monopoles, one with positive and one with negative vorticity, are placed in the arrangement given by Eq. (22). Although both initial monopoles have a linear ω,ψ-relation, the combination does not have a single linear ω,ψ-relation. Since the initial vorticity distribution is rather smooth, the vorticity fluctuations as seen in Fig. 12 are in this case considerably smaller. Again a Lamb-like dipole is formed, but it takes more time than it takes for the dipole of Eq. (22) at the same distance d. Where the origin of this difference lies is not immediately clear. For dipole Eq. (22) with its step-wise initial vorticity distribution both nonlinear and viscous effects are stronger than for the much smoother Bessel-type monopoles. As a result of this the spreading of the vorticity for dipole Eq. (22) towards a circular form is faster and it assumes Lamb-like characteristics quicker than the dipole with initially Bessel-type elliptic monopoles does.

6. Concluding remarks

If a Lamb dipole is placed at the centre of a finite, rectangular domain with its axis parallel to the boundaries at $y=\pm y_w$, then the dipole's velocity U is lower the narrower the domain is. If viscosity is present the vorticity of the dipole is gradually spread over a larger area, i.e. the radius a of the dipole increases as time evolves. At the same time the vorticity extrema decrease, as a result of which the dipole's velocity decreases.

The Lamb dipole initially has a linear relation between vorticity ω and streamfunction ψ, namely $\omega=k^2\psi$, where the value of k follows from $ak\approx 3.8317$. As the dipole moves and grows, the ω,ψ-relation becomes nonlinear, at first near the edge and the axis of the dipole, but as time goes on the nonlinearity spreads towards the vorticity extrema. As long as there is still a linear part in the ω,ψ-relation around the extrema of vorticity, a k-value can be found. It appears that k decreases as function of time, but the product ak increases with time. During this evolution the dipole retains its major characteristics: a more or less circular form and a more or less linear ω,ψ-relation. These characteristics are named "Lamb-like".

As the dipole evolves further, a larger and larger part of the ω,ψ-relation becomes nonlinear, until finally the entire ω,ψ-relation can be described by $\omega=C\sinh(2\psi)$ for a certain constant C, which depends only on time. The dipole has then lost its main Lamb-like characteristics, although it is still circular to within a few per cent. The time scale at which this process takes place is determined mainly by the strength of the viscous effects; it does not so much depend on the strength of the initial dipole (a stronger initial dipole only moves faster).

Since the Lamb dipole appears to retain its characteristics for a long time, tests have been done with other 2D dipolar vorticity structures as initial vorticity distribution. The alternative dipoles studied have the same symmetry property as the Lamb dipole: two patches of oppositely signed vorticity which lie symmetrically about the line of motion. These dipoles evolve into a Lamb-like dipole, followed by a decay like that of the Lamb dipole itself. The time it takes to form a Lamb-like dipole depends on the initial vorticity distribution: the further it is away from a Lamb dipole, the more time it takes.

The main conclusion, therefore, is that a dipolar vortex with Lamb-like characteristics is a very stable vorticity structure in a viscous finite fluid, and initial vorticity distributions that are not too different from a Lamb dipole evolve to a dipolar structure with Lamb-like characteristics.

Acknowledgements

The authors wish to thank H.J.H. Clercx for useful discussions and suggestions regarding some numerical aspects, and the referees for their constructive remarks. The research described in this paper was carried out when JHGMvG was working at the Fluid Dynamics Laboratory in Eindhoven on a research project financed by the Netherlands Organisation for Scientific Research (NWO) programme Non-Linear Systems. The authors gratefully acknowledge this support.

References

Arakawa, A., 1966. Computational design for long-term numerical integration of the equations of fluid motion: two-dimensional incompressible flow. Part I. J. Comput. Phys. 1, 119–143.

Chaplygin, S.A., 1903. One case of vortex motion in fluid. Trans. Phys. Sect. Imperial Moscow Soc. Friends of Natural Sci. 11 (2), 11–14. Also in Collected Works, 1948, vol. 2, pp. 155–165 (in Russian).

Couder, Y., Basdevant, C., 1986. Experimental and numerical study of vortex couples in two-dimensional flows. J. Fluid Mech. 173, 225–251.

Dritschel, D.G., 1988. Nonlinear stability bounds for inviscid, two-dimensional, parallel or circular flows with monotonic vorticity, and the analogous three-dimensional quasi-geostrophic flows. J. Fluid Mech. 191, 575–581.

Flór, J.B., Van Heijst, G.J.F., 1994. An experimental study of dipolar vortex structures in a stratified fluid. J. Fluid Mech. 279, 101–133.

Flór, J.B., Van Heijst, G.J.F., Delfos, R., 1995. Decay of dipolar vortex structures in a stratified fluid. Phys. Fluids 7, 374–383.

Joyce, G., Montgomery, D., 1973. Negative temperature states for the two-dimensional guiding-centre plasma. J. Plasma Phys. 10, part 1, 107–121.

Lamb, H., 1932. Hydrodynamics, 6th ed. Cambridge University Press, Cambridge.

Legras, B., Santangelo, P., Benzi, R., 1988. High-resolution numerical experiments for forced two-dimensional turbulence. Europhys. Lett. 5, 37–42.

McWilliams, J.C., 1984. The emergence of isolated coherent vortices in turbulent flow. J. Fluid Mech. 146, 21–43.

Meleshko, V.V., Van Heijst, G.J.F., 1994. On Chaplygin's investigations of two-dimensional vortex structures in an inviscid fluid. J. Fluid Mech. 272, 157–182.

Montgomery, D., Matthaeus, W.H., Stribling, W.T., Martinez, D., Oughton, S., 1992. Relaxation in two dimensions of the 'sinh-Poisson' equation. Phys. Fluids A 4, 3–6.

Nguyen Duc, J.-M., Sommeria, J., 1988. Experimental characterization of steady two-dimensional vortex couples. J. Fluid Mech. 192, 175–192.

Nielsen, A., Juul Rasmussen, J., 1997. Formation and temporal evolution of the Lamb-dipole. Phys. Fluids 9, 982–991.

Orlandi, P., 1990. Vortex dipole rebound from a wall. Phys. Fluids A 2, 1429–1436.

Pasmanter, R., 1993. A solution equation and most probable states of inviscid, incompressible 2D flows. In: Kida, S. (Ed.), Unstable and Turbulent Motion of Fluid. World Scientific, Singapore, pp. 302–310.

Swaters, G.E., 1991. Dynamical characteristics of decaying Lamb couples. J. Appl. Math. Phys. (ZAMP) 42, 109–121.

Terazawa, K., 1922. On the decay of vortical motion in a viscous fluid. Report of the Aeronautical Research Institute – Tôkyô Imp. Univ. 1, No. 4.

Trieling, R.R., Van Wesenbeeck, B., Van Heijst, G.J.F., 1997. Dipolar vortices in a strain flow. Phys. Fluids, submitted.

Van Heijst, G.J.F., Flór, J.B., 1989. Dipole formation and collisions in a stratified fluid. Nature 340, 212–215.

Velasco Fuentes, O.U., Van Heijst, G.J.F., 1994. Experimental study of dipolar vortices on a topographic β-plane. J. Fluid Mech. 259, 79–106.

Verzicco, R., Flór, J.-B., Van Heijst, G.J.F., Orlandi, P., 1995. Numerical and experimental study of the interaction between a vortex dipole and a circular cylinder. Exp. Fluids 18, 153–163.